Are spectroscopic factors from transfer reactions consistent with asymptotic normalization coefficients?

D. Y. Pang
School of Physics and MOE Key Laboratory of Heavy Ion Physics, Peking University, Beijing, People's Republic of China
National Superconducting Cyclotron Laboratory and Department of Physics and Astronomy, Michigan State University, East Lansing, Michigan 48864, USA

F. M. Nunes*
National Superconducting Cyclotron Laboratory and Department of Physics and Astronomy, Michigan State University, East Lansing, Michigan 48864, USA

A. M. Mukhamedzhanov†
Cyclotron Institute, Texas A&M University, College Station, Texas 77843, USA
(Received 25 May 2006; published 1 February 2007)

It is extremely important to devise a reliable method to extract spectroscopic factors from transfer cross sections. We analyze the standard DWBA procedure and combine it with the asymptotic normalization coefficient, extracted from an independent data set. We find that the single particle parameters used in the past generate inconsistent asymptotic normalization coefficients. In order to obtain a consistent spectroscopic factor, nonstandard parameters for the single particle overlap functions can be used but, as a consequence, often reduced spectroscopic strengths emerge. Different choices of optical potentials and higher order effects in the reaction model are also studied. Our test cases consist of ^{14}C$(d, p)^{15}$C(g.s.) at $E_d^{\rm lab} = 14$ MeV, ^{16}O$(d, p)^{17}$O(g.s.) at $E_d^{\rm lab} = 15$ MeV and ^{40}Ca$(d, p)^{41}$Ca(g.s.) at $E_d^{\rm lab} = 11$ MeV. We underline the importance of performing experiments specifically designed to extract asymptotic normalization coefficients for these systems.

DOI: 10.1103/PhysRevC.75.024601 PACS number(s): 21.10.Jx, 24.10.−i, 24.50.+g, 25.40.Hs

I. INTRODUCTION

The shell model formalism first introduced spectroscopic factors (SF) to describe the shell occupancy [1]. In particular, $S_{lj}^{f,i}$, the single particle SF, is defined as the norm of the overlap function of a nucleus $(A + 1)$ in a particular state i with a nucleus A in a state f, where the valence nucleon is in an orbital with orbital and total angular momentum (l, j). These SFs have been extensively compared with those extracted from reactions. At present *ab initio* calculations are improving the accuracy of the calculated SFs (e.g., [2,3]). One would eventually like to have a very accurate probe that could test the predictions of these models and could disentangle the relevant elements of the *NN* force that are still missing, especially when moving toward the driplines.

From the experimentalist point of view, a spectroscopic factor is a ratio of measured to predicted differential cross sections. Phenomenological spectroscopic factors are extensively used in a variety of topics, from nuclear reactions to astrophysics or applied physics, yet the procedure for their extraction from the data has remained essentially the same for decades. Most of the work in the 1960s and 1970s used direct transfer reactions, such as (d, p), (d, t), $(^3\text{He}, d)$, $(^3\text{He}, \alpha)$, as the central tool [4–6]. However transfer analyses have a reputation of large uncertainties.

Other methods to extract spectroscopic information include the $(e, e'p)$ reactions or the nuclear knockout in inverse kinematics. For stable nuclei, there have been many electron knockout experiments. They have provided SFs with rather small error bars [7]. The analysis of these measurements along a wide mass range, for single particle states with expected SFs close to unity, show an overall reduction of the SF ($\approx$0.6). The source of this reduction is not yet well understood [8] although one expects *NN* short or long range correlations which are not included in the present day non *ab initio* shell model to contribute.

Nuclear knockout in inverse kinematics using radioactive beams is a new probe introduced at the National Superconducting Cyclotron Laboratory [9]. A systematic study of spectroscopy on a variety of nuclei, ranging from the stability valley to the proton dripline, have been performed using this technique. It is found that the measured spectroscopic factors suffer from a reduction relative to the shell model predictions and the reduction factor changes with binding energy [10]. Again, it is not clear where this quenching [1] comes from. Of course, as $(e, e'p)$, this technique is only suitable for studying the single particle structure of the ground states of nuclei.

The $(e, e'p)$ cross section is sensitive to the structure all the way to the inside of the nucleus, whereas the transfer is typically peripheral and surface peaked. The knockout reactions with radioactive beams have been performed in a kinematical regime where the eikonal approximation can be used, to simplify the reaction theory and to reduce the reaction model uncertainties [6]. Nuclear knockout results [1] are in agreement with the $(e, e'p)$ SFs for the tested stable closed shell nuclei [11]. Transfer and $(e, e'p)$ have also been compared [7] for ^{48}Ca. Earlier transfer studies

*Electronic address: nunes@nscl.msu.edu
†Electronic address: akram@comp.tamu.edu

provided a spectroscopic factor for the last proton close to unity, but a reanalysis by [7] including finite-range and nonlocal effects in the transfer reaction model, show that the transfer result can be brought down to 0.6, the $(e, e'p)$ value.

The spectroscopic factor is the norm of the overlap function, which peaks well inside the nuclear radius R_N. As the $(e, e'p)$ reaction can probe the nuclear interior, it is suitable for extracting SFs as long as the reaction mechanism is well understood. However there are some problems with the high momentum transfer component, associated with probing the inside of the nucleus, because then the Born approximation is not valid [12]. For exotic nuclei near or on the driplines, transfer reactions are a unique tool and, hence, can have a large impact in the programs of the new generation rare isotope laboratories.

The standard framework for analysing transfer data with the intent of extracting SFs is the distorted-wave Born approximation (DWBA). Overall, it has been very successful in describing angular distributions at forward angles and less so for the larger angles where higher order become more important. The SF is the normalization needed for the calculated DWBA differential cross section to match the experimental one at forward angles (e.g., [13–15]). The uncertainty of the extracted SF resulting from the normalization of the DWBA cross section is assumed to be $\sim$30%, even if the statistical errors are low. The reasons for this inaccuracy are typically attributed to ambiguities in the optical potentials, the inadequacy of the DWBA reaction theory, or the dependence on the single-particle potential parameters. Recently, systematic studies on ^{12}C$(d, p)^{13}$C have shown that it is possible to bring SFs into conformity using a global optical potential prescription [16,17], whereas arbitrary choices of the optical potential will hold disparate results. As to the reaction mechanism, there are many studies on the validity of DWBA (e.g., [18]) and typically the reaction mechanism needs to be checked case by case. In addition, Hartree-Fock densities have been suggested as a mean to constrain the single particle parameters [19]. Therein, the single particle radii for the Ca isotopes were adjusted to reproduce the known rms matter radii, and zero range DWBA calculations were performed to extract the SFs.

In [20], a combined method of extracting SFs from transfer reactions was introduced. This method can also be applied to breakup and $(e, e'p)$ reactions. The combined method, which is based on the introduction of the asymptotic normalization coefficients (ANC) into the transfer analysis, allows one to significantly reduce the uncertainty in the choice of the bound state potential parameters and to test the DWBA or other underlying reaction theory. In the combined method the ANC should be determined from an independent measurement of a peripheral reaction while the SF is determined from transfer reactions which are sensitive to the nuclear interior. In [20] we emphasize that fixing the ANC is absolutely necessary, since even when the beam energy is well above the Coulomb barrier, most of the reaction happens in the asymptotic region. It has been found [20] that, in (d, p) reactions, the standard single particle parameters for the radius $r_0 = 1.2$ fm and diffuseness $a = 0.65$, which typically provide unit SF for closed shell nuclei, do not reproduce the value of the ANC extracted from the lower energy measurement. In this work we expand on the ideas of the combined method, and explore other uncertainties (such as optical potentials and higher order effects) to attempt a unification of the SF and the ANC, searching for a reaction description which is practical and gives reliable spectroscopic information.

In Sec. II we present a short description of the theoretical framework. In Sec. III we detail the results for our three test cases: DWBA results using a global deuteron optical potential, DWBA results where the deuteron potential is obtain from a direct fit to the elastic, for results including deuteron breakup within the adiabatic model, checks of other higher order effects and also in a further analysis of peripherality. Finally, a discussion of the results and conclusions are drawn in Sec. IV.

II. REACTION FORMALISM AND SPECTROSCOPY

The central element of the analysis of the transfer reaction $A(d, p)B$ [20] is the overlap function $I^B_{An}(\mathbf{r})$ between bound states of nuclei $B = A + n$ and A which depends on $\mathbf{r}$, the radius-vector connecting the center of mass of A with n. The square norm of the overlap function gives a model-independent definition of the SF. It is important to keep in mind that most of the contribution to the SF comes from the interior.

The radial overlap function (for $B = A + n$) behaves as a spherical Bessel function for large distances:

$$I^B_{An(lj)}(r) \overset{r>R_N}{\approx} C_{lj}\, i\,\kappa\, h_l(i\,\kappa\, r). \tag{1}$$

Here, $\kappa = \sqrt{2\,\mu_{An}\,\varepsilon_{An}}$, where ε_{An} is the binding energy for $B \to A + n$, and μ_{An} is the reduced mass of A and n. R_N represents a radius beyond which the nuclear potential is negligible and C_{lj} is referred to as the asymptotic normalization coefficient (ANC).

The standard practice is to take the radial dependence of the overlap function from the single particle orbital. This radial wave function is usually generated by a Woods-Saxon potential with a given geometry. The depths are adjusted such that the single particle orbital has the correct separation energy and quantum numbers (n, l, j). Generally, the single particle orbital has the same asymptotic behavior as the many-body overlap function:

$$\varphi_{An(n_r lj)}(r) \overset{r>R_N}{\approx} b_{n_r lj}\, i\,\kappa\, h_l(i\,\kappa\, r), \tag{2}$$

where $b_{n_r lj}$ is the single-particle ANC (SPANC). From the relations in Eqs. (1) and (2), and under the assumption that the many-body overlap is indeed proportional to the single particle function all the way down to $r = 0$, the ANC and the SF are related by $C^2_{lj} = S_{n_r lj}\, b^2_{n_r lj}$. So far, it is hard to check the exactness of this proportionality given the accuracy of the asymptotics of the wave function obtained from *ab initio* calculations.

For $A(d, p)B$, the one-step post-form finite range DWBA amplitude is given by

$$M = \left\langle \psi^{(-)}_f I^B_{An} \middle| \Delta V | \varphi_{pn}\, \psi^{(+)}_i \right\rangle, \tag{3}$$

where $\Delta V = V_{pn} + V_{pA} - U_{pB}$ is the transition operator, V_{ij} is the interaction potential between i and j, and U_{pB} is the optical potential in the final state. $\psi_i^{(+)}$ and $\psi_f^{(-)}$ are the distorted waves in the initial and final states and φ_{pn} is the deuteron bound-state wave function.

In [20], the reaction amplitude is split into interior and exterior parts. The normalization of the former is determined by the SF while the ANC governs the normalization of the latter. We introduce the ratio $R^{\rm th}(b_{n_r lj}) = \frac{\sigma^{\rm th}(\theta_{\rm peak})}{b^2_{n_r lj}}$ to compare with the experimental counterpart $\mathcal{R}^{\rm exp} = \frac{\sigma^{\rm exp}(\theta_{\rm peak})}{(C^{\rm exp}_{lj})^2}$. Introducing the information about the ANC fixes the exterior contribution. If the reaction is completely peripheral, its cross section will scale directly as C^2_{lj}, but will hold no information on the SF. If there is an interior contribution, the theoretical cross section has a nontrivial dependence on the SPANC $b_{n_r lj}$ which can be constrained by $R^{\rm th}(b_{n_r lj}) = \mathcal{R}^{\rm exp}$. Hence, peripheral reactions are ideal to extract ANCs but useless for extracting SFs. To determine SFs one should explore nonperipheral reactions.

The combined method presented in [20] tries to isolate the ambiguity coming from the single particle parameters but the resulting SFs are often smaller than those produced by shell model. As in this method, the interior part plays an important role to determine the SF, the results will be more sensitive to the optical potentials and coupling effects. With global optical potentials, the single particle parameters obtained from $R^{\rm th}(b_{n_r lj}) = \mathcal{R}^{\rm exp}$ are often far from the conventional values, and the corresponding angular distributions provide a worse description of the data, when compared to the standard procedure. The main questions we want to address here is whether DWBA (or higher order reaction theory) allows us to extract correct SFs when fixing the peripheral part of the transfer amplitude through the experimentally determined ANCs.

III. RESULTS

The most important consequence of the work in [20] is the fact that within the standard DWBA approach, the extracted spectroscopic factors are inconsistent with the ANCs obtained through independent measurements. This will be illustrated through the examples in this section.

By *standard DWBA* we mean the framework in which the one-step transfer matrix element is evaluated with incoming and outgoing distorted waves calculated by fitting the deuteron and proton elastic scattering with local optical potentials. The transfer operator contains finite range effects as well as the full complex remnant term.

ANCs can be extracted from sub-Coulomb reactions, which are Coulomb dominated and contain virtually no contribution from the nuclear interior. For the ^{17}O(g.s.) case, we have two sets of heavy ion collision data that provide $C^2_{d5/2} = 0.67 \pm 0.05$ fm^{-1} [21] and $C^2_{d5/2} = 0.69 \pm 0.03$ fm^{-1} [22], respectively. For the other two cases, no heavy ion transfer data exist, therefore alternative data were used. For ^{15}C(g.s.) knockout data from [23] and [24] were jointly used in [25] to extract an ANC of $C^2_{s1/2} = 1.48 \pm 0.18$ fm^{-1}. Note that other values can be obtained through different types of reactions such as capture [26]. We want to be consistent with the ANC extractions in all three test cases, thus we use the ANC obtained through nuclear processes. For ^{41}Ca(g.s.), (d, p) data at sub-Coulomb energies was used [27] from which we obtain $C^2_{f7/2} = 8.36 \pm 0.42$ fm^{-1}.

The transfer calculations are performed for ^{14}C(d, p) ^{15}C(g.s.) at $E_d^{\rm lab} = 14$ MeV [32], ^{16}O$(d, p)^{17}$O(g.s.) at $E_d^{\rm lab} = 15$ MeV [33], and ^{40}Ca$(d, p)^{41}$Ca(g.s.) at $E_d^{\rm lab} = 11$ MeV [34]. These reactions were chosen because both elastic and transfer data exist at the same energy. All data can be found on the database website at Michigan State University [35]. Calculations were performed with the code FRESCO [36].

A. DWBA with global deuteron potential

We perform finite-range post-form DWBA calculations, including the full complex transition operator ΔV. The Reid-soft-core interaction [30] is used for the deuteron ground state wave function, and includes both S- and D-waves. We use the central part of the Reid-soft-core interaction for V_{np} in the transfer operator. The diffuseness of the single particle orbital of the final state is kept fixed ($a = 0.65$ fm), but the radius is varied to generate a range of SPANCs. Throughout this work we will always use the CH89 global parametrization [28] for the outgoing distorted waves. We have checked that by using a different proton global potential, spectroscopic factors change less than 10%. We will look into several approaches to determine the initial wave function. In this subsection we take the Perey and Perey deuteron potential (PP) [31].

The resulting angular distributions are displayed in Figs. 1, 2, and 3, for a subset of r_0, and compared to data. We will refer to these calculation as DWBAg. Even though it provides a fair description of the first peak of the distribution, it is inadequate for the large angles, where higher order effects become important. This is a well-known characteristic of DWBA.

For each single particle radius r_0 of $B = A + n$, the normalization of the first transfer peak is used to determine the spectroscopic factor, and the ANCs are obtained directly from $C^2_{lj} = S_{n_r lj}\, b^2_{n_r lj}$. Results are presented in Table I. If one takes the standard radius of 1.21 fm, one can see that the extracted SFs are all close to unity, but none of the ANCs are consistent with the values extracted from experiment, with the most serious mismatch for ^{41}Ca, nearly a factor of 2. Knockout measurements suggest that in ^{17}O and ^{41}Ca

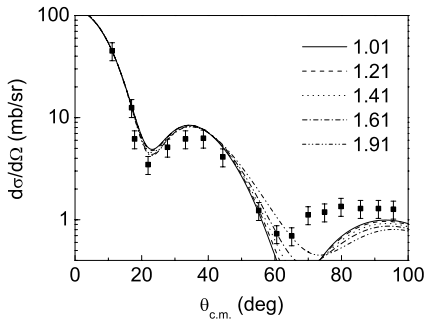

FIG. 1. ^{14}C$(d, p)^{15}$C at $E_d = 14$ MeV with a global deuteron potential (DWBAg). Data from [32].

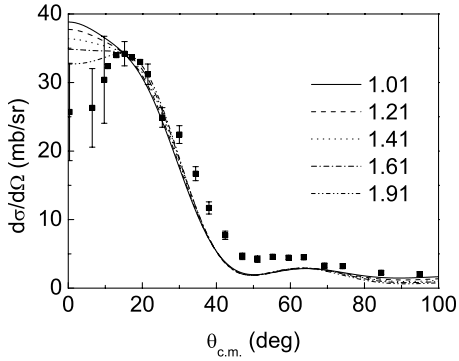

FIG. 2. ^{16}O(d, p)^{17}O at $E_d = 15$ MeV with a global deuteron potential (DWBAg). Data from [33].

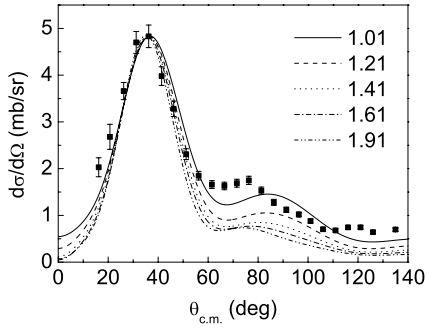

FIG. 3. ^{40}Ca(d, p)^{41}Ca at $E_d = 11$ MeV with a global deuteron potential (DWBAg). Data from [34].

there is a reduction of the SF to ≈ 0.6. One can see from Table I, that this SF is reproduced at $r_0 \approx 1.4$ fm for ^{17}O and $r_0 \approx 1.3$ fm for ^{41}Ca, but the SF/ANC inconsistency is not resolved.

Finite range effects are known to be important in (d, p) reactions, but remnant contributions are often assumed to be small. We have repeated DWBAg calculations excluding the remnant term and find that indeed, remnant contributions are insignificant for the reactions of ^{14}C and ^{16}O, but can contribute up to 30% for the ^{40}Ca(d, p) reaction.

B. DWBA with fitted deuteron potential

The elastic channel data are also available for the three reactions under scrutiny, ^{14}C(d, p)^{15}C(g.s.) at $E_d^{\rm lab} = 14$ MeV, ^{16}O(d, p)^{17}O(g.s.) at $E_d^{\rm lab} = 15$ MeV and ^{40}Ca(d, p)^{41}Ca(g.s.) at $E_d^{\rm lab} = 11$ MeV. We have repeated this study using optical potentials fitted specifically to the corresponding elastic data, using FRESCO [36]. The optical potentials resulting from the elastic fits are presented in Table II and differ somewhat from the global compilations. The resulting transfer cross sections, together with the corresponding elastic scattering, are shown in Figs. 4, 5, and 6. We will refer to these calculations as DWBAf. For both the ^{14}C(d, p) and the ^{41}Ca(d, p) reactions, the SF/ANC inconsistency remains whereas for the ^{16}O(d, p) a spectroscopic factor of 0.6–1 produces ANCs much closer to the value extracted from a sub-Coulomb measurement. This can be seen from Table III where SPANCs, SFs, and ANCs are presented as a function of the single particle radius for the three reactions under study.

C. Adiabatic deuteron potential

It is well known that the deuteron breakup can have an effect on the transfer cross sections. One way to take this into account would be to couple explicitly the deuteron continuum within the continuum discretized coupled channel (CDCC) method [39]. The complexity of the procedure would not be practical for the general experimental community. Alternatively, the adiabatic method developed by Johnson and Soper [29] can be used to describe the entrance channel and obtain the transfer cross section while including the deuteron breakup channel. This procedure is by far simpler than the CDCC approach and can easily be used in systematic studies (e.g., [16,17]). The three-body wave function for the d-T system obtained with the adiabatic approximation has the correct properties in the range of V_{np} yet should not be used in the asymptotic region. For this reason we perform finite range calculations but do not include the remnant term in Eq. (3). Also important is that

TABLE I. SFs and ANCs obtained from DWBA analyses: Perey and Perey potential for the deuteron.

r_0 (fm)	^{14}C (14 MeV)			^{16}O (15 MeV)			^{40}Ca (11 MeV)		
	b (fm^{-1})	SF	C^2 (fm^{-1})	b (fm^{-1})	SF	C^2 (fm^{-1})	b (fm^{-1})	SF	C^2 (fm^{-1})
1.01	1.342	1.40	2.516	0.675	1.54	0.700	1.322	1.66	2.900
1.11	1.377	1.33	2.527	0.753	1.28	0.723	1.664	1.18	3.273
1.21	1.415	1.27	2.541	0.841	1.05	0.745	2.091	0.834	3.647
1.31	1.454	1.21	2.554	0.940	0.869	0.767	2.623	0.583	4.018
1.41	1.496	1.15	2.572	1.050	0.716	0.789	3.283	0.407	4.390
1.51	1.540	1.09	2.592	1.173	0.589	0.811	4.099	0.284	4.775
1.61	1.586	1.04	2.621	1.310	0.486	0.833	5.107	0.199	5.198
1.71	1.635	0.995	2.659	1.462	0.401	0.857	6.347	0.141	5.682
1.81	1.686	0.953	2.710	1.631	0.332	0.883	7.872	0.101	6.260
1.91	1.740	0.918	2.777	1.818	0.275	0.911	9.744	0.073	6.968
	$C^2_{\rm exp}$		1.48 ± 0.18 fm^{-1}	$C^2_{\rm exp}$		0.67 ± 0.05 fm^{-1}	$C^2_{\rm exp}$		8.36 ± 0.42 fm^{-1}

TABLE II. Deuteron optical potential parameters resulting from the fit to elastic data (fit 1).

A	E_{beam} (MeV)	V_R (MeV)	R_R (fm)	a_R (fm)	W_d(MeV)	R_I (fm)	a_I (fm)	V_{so}(MeV)	R_{so} (fm)	a_{so} (fm)
14	14	92.880	1.1486	0.596	3.848	1.085	1.347	9.164	0.883	0.244
16	15	115.911	1.017	0.846	11.257	1.073	0.584	11.600	0.578	0.343
40	11	115.177	1.040	0.712	5.287	1.375	0.856	4.486	0.382	0.266

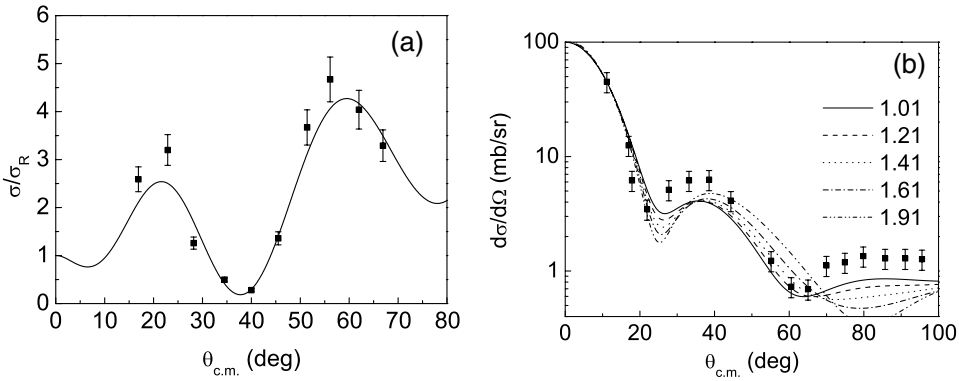

FIG. 4. (a) Elastic scattering fit $^{14}\text{C} + d$; (b) $^{14}\text{C}(d, p)^{15}\text{C}$ at $E_d = 14$ MeV with a fitted deuteron potentials (DWBAf). Both elastic and transfer data from [32].

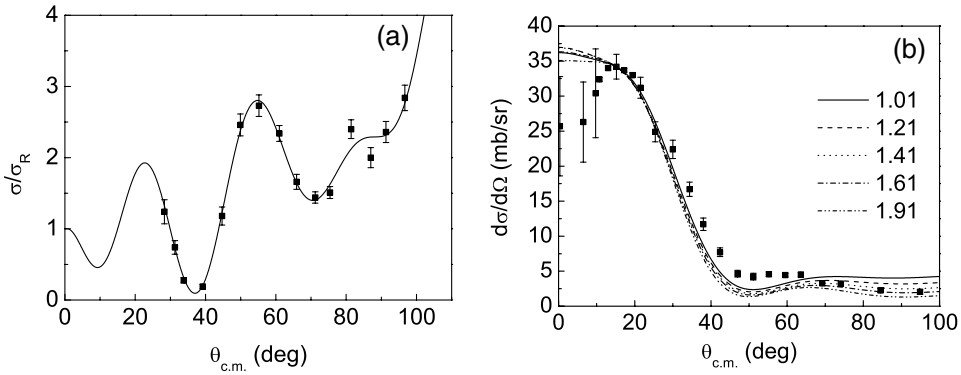

FIG. 5. (a) Elastic scattering fit $^{14}\text{C} + d$; (b) $^{16}\text{O}(d, p)^{17}\text{O}$ at $E_d = 15$ MeV with a fitted deuteron potentials (DWBAf). Elastic data from [37] and transfer data from [33].

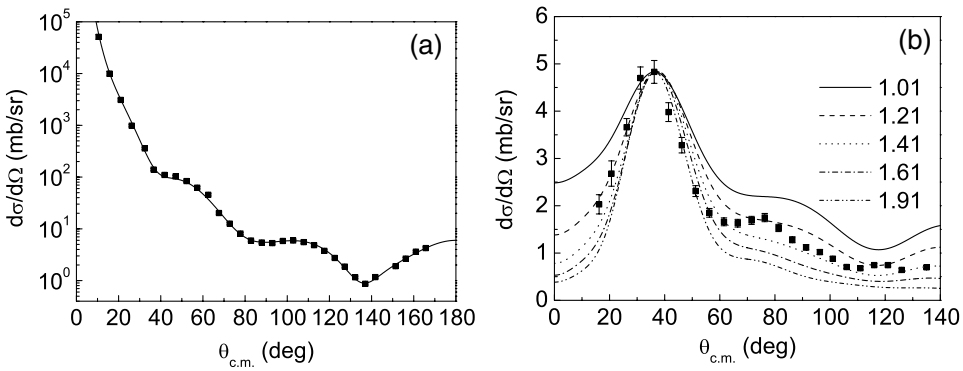

FIG. 6. (a) Elastic scattering fit $^{14}\text{C} + d$; (b) $^{40}\text{Ca}(d, p)^{41}\text{Ca}$ at $E_d = 11$ MeV with a fitted deuteron potentials (DWBAf). Elastic data from [38] and transfer data from [34].

TABLE III. SFs and ANCs obtain from DWBA analyses: deuteron optical potential directly fitted to the corresponding elastic data.

r_0 (fm)	^{14}C (14 MeV)			^{16}O (15 MeV)			^{40}Ca (11 MeV)		
	b (fm^{-1})	SF	C^2 (fm^{-1})	b (fm^{-1})	SF	C^2 (fm^{-1})	b (fm^{-1})	SF	C^2 (fm^{-1})
1.01	1.34	1.50	2.70	0.67	1.38	0.632	1.32	1.23	2.159
1.11	1.37	1.42	2.70	0.75	1.09	0.622	1.66	0.985	2.729
1.21	1.41	1.35	2.71	0.84	0.869	0.616	2.09	0.748	3.272
1.31	1.45	1.27	2.70	0.93	0.693	0.613	2.62	0.545	3.754
1.41	1.49	1.20	2.69	1.04	0.555	0.613	3.28	0.387	4.172
1.51	1.54	1.13	2.68	1.17	0.447	0.617	4.10	0.271	4.557
1.61	1.58	1.05	2.66	1.31	0.363	0.625	5.11	0.189	4.945
1.71	1.63	0.988	2.64	1.46	0.297	0.636	6.35	0.133	5.380
1.81	1.68	0.921	2.62	1.63	0.244	0.651	7.87	0.095	5.904
1.91	1.74	0.859	2.60	1.81	0.202	0.671	9.75	0.069	6.555
	$C^2_{\rm exp}$		1.48 ± 0.18 fm^{-1}	$C^2_{\rm exp}$		0.67 ± 0.05 fm^{-1}	$C^2_{\rm exp}$		8.36 ± 0.42 fm^{-1}

the deuteron wave function be an eigenstate of V_{np} used in the transfer operator. Transfer matrix elements with the full RSC potential are not simple. Thus we have used the central gaussian, refitted to reproduce the correct binding energy and the same D as the RSC potential, for calculating both, the wave function and the transfer operator.

We use the CH89 nucleon potential for the U_{nT} and U_{pT} at half the deuteron incident energy and calculate the adiabatic potential using the parametrization in [40] which included finite range corrections. We will refer to these results as the adiabatic wave approximation (ADWA) [41]. The cross section obtained for the three reactions under study are presented in Figs. 7–9. In Table IV we show the results for the extracted SF and corresponding ANCs. An overall reduction of the spectroscopic factors is observed. The angular distributions show some improvement as compared to those within DWBAg or DWBAf. However, it becomes clear that deuteron breakup is unable to remove the inconsistency between SF and ANC, specially in the ^{41}Ca case, where a persistent factor of 2 remains.

As mentioned above, the ADWA results here presented do not include the remnant. Results from DWBAg show that remnant contributions are not important for the lighter cases under study. Even though remnant contributions to ^{40}Ca(d, p)^{41}Ca are not negligible, the magnitude is much smaller than the mismatch observed and we do not expect their inclusion within ADWA would change the conclusions. Also, the deuteron wave function for the adiabatic calculations is s-wave only (does not contain the d-wave and the tensor interaction). This effect alone reduces the spectroscopic factors by $\approx$10%. However our conclusions, namely that deuteron breakup cannot account for the inconsistency between SF and ANC, remain.

D. Other higher order effects

The transfer couplings for the examples we are studying are relatively strong, therefore one solution to the inconsistency between SF and ANC could reside in higher order processes

TABLE IV. SFs and ANCs obtained from ADWA analyses.

r_0 (fm)	^{14}C (14 MeV)			^{16}O (15 MeV)			^{40}Ca (11 MeV)		
	b (fm^{-1})	SF	C^2 (fm^{-1})	b (fm^{-1})	SF	C^2 (fm^{-1})	b (fm^{-1})	SF	C^2 (fm^{-1})
1.01	1.34	1.16	2.08	0.67	1.45	0.659	1.32	1.80	3.14
1.11	1.37	1.11	2.10	0.75	1.19	0.675	1.66	1.30	3.57
1.21	1.41	1.06	2.12	0.84	0.974	0.688	2.09	0.895	3.92
1.31	1.45	1.01	2.14	0.93	0.794	0.701	2.62	0.609	4.19
1.41	1.49	0.969	2.17	1.04	0.646	0.712	3.28	0.410	4.43
1.51	1.54	0.928	2.20	1.17	0.526	0.724	4.10	0.278	4.67
1.61	1.58	0.891	2.24	1.31	0.429	0.737	5.11	0.189	4.94
1.71	1.63	0.858	2.30	1.46	0.351	0.751	6.35	0.131	5.28
1.81	1.68	0.830	2.36	1.63	0.289	0.768	7.87	0.092	5.72
1.91	1.74	0.807	2.44	1.81	0.238	0.788	9.75	0.066	6.30
	$C^2_{\rm exp}$		1.48 ± 0.18 fm^{-1}	$C^2_{\rm exp}$		0.67 ± 0.05 fm^{-1}	$C^2_{\rm exp}$		8.36 ± 0.42 fm^{-1}

TABLE V. Variation of the SFs and the ANCs with r_0 for CCBA calculations of $^{16}O(d, p)^{17}O$ at $E_d = 15$ MeV.

$r0$	SF	$b(1d5/2)$	$C^2(d5/2)$
1.16	1.28	0.6795	0.59
1.20	1.17	0.7003	0.58
1.24	1.08	0.7215	0.56
1.28	0.99	0.7430	0.55
1.32	0.92	0.7647	0.53

TABLE VI. Variation of the SFs and the ANCs with r_0 for CCBA calculations of $^{40}Ca(d, p)^{41}Ca$ at $E_d = 11$ MeV.

$r0$	SF	$b(1f7/2)$	$C^2(f7/2)$
1.22	1.16	1.7869	3.69
1.24	1.09	1.8541	3.75
1.26	1.03	1.9233	3.81
1.28	0.97	1.9944	3.85
1.30	0.91	2.0674	3.88

TABLE VII. Single particle orbitals adjusted to produce the experimental ANC, when SF is unity.

	^{15}C	^{17}O	^{41}Ca
r_0 (fm)	1.10	1.25	1.30
a (fm)	0.52	0.60	0.75
C^2 (fm$^{-1)}$	1.62	0.68	8.24
R_{rms}(fm)	5.1	3.5	4.2

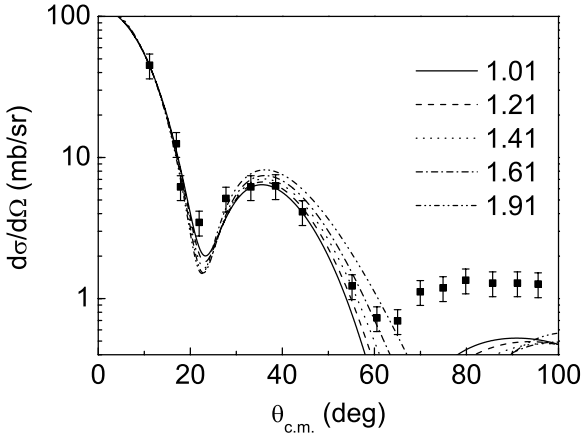

FIG. 7. $^{14}C(d, p)^{15}C$ at $E_d = 14$ MeV with ADWA. Data from [32].

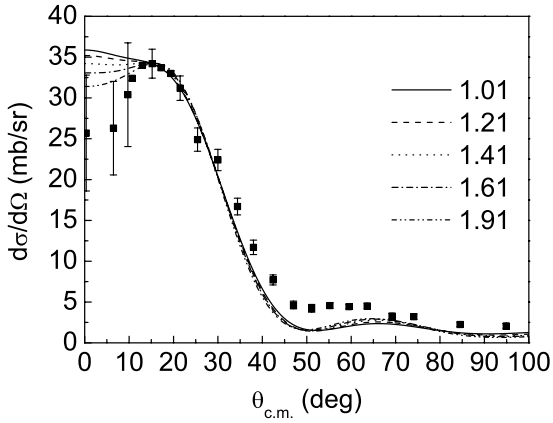

FIG. 8. $^{16}O(d, p)^{17}O$ at $E_d = 15$ MeV with ADWA. Data from [33].

in the reaction mechanism, other than deuteron breakup. In these calculations our starting point is DWBAf. First we consider multiple transfer couplings within the coupled reaction channel approach (CRC). Note that some of these effects are accounted for within ADWA. We restrict ourselves to the (d, p) transfer coupling connecting ground states of A and B. For all three reactions, we increase the number of iterations until convergence is achieved. We refit the deuteron optical potentials, so that the elastic scattering is still well reproduced.

(i) For $^{14}C(d, p)^{15}C$(g.s.) at $E_d^{lab} = 14$ MeV, we find that there is a significant effect of higher order transfer couplings in the cross section, which amounts to a reduction of the required SF. Still this does not completely solve the inconsistency. For example, for $r_0 = 1.3$ fm, $S = 1.013$, and $C^2 = 2.14$ fm^{-1}.

(ii) CRC effects for $^{16}O(d, p)^{17}O$ at 15 MeV are weak (a few percent).

(iii) For $^{40}Ca(d, p)^{41}Ca$ at 11 MeV, CRC increases the transfer cross section by $\approx$20% which produces lower SFs. This makes the inconsistency SF/ANC more severe.

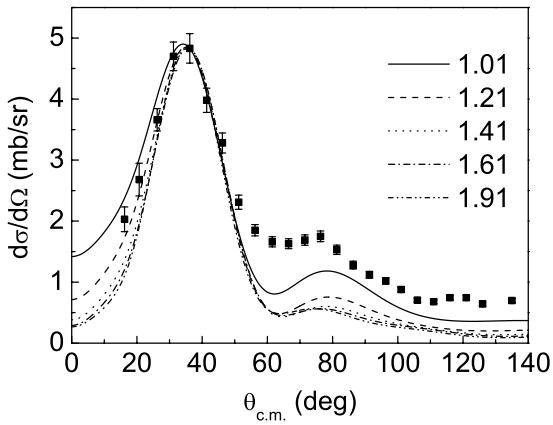

FIG. 9. $^{40}Ca(d, p)^{41}Ca$ at $E_d = 11$ MeV with ADWA. Data from [34].

TABLE VIII. Deuteron optical potential parameters resulting from the simultaneous fit to elastic and transfer data.

A	E_{beam} (MeV)	V_R (MeV)	R_R (fm)	a_R (fm)	W_d(MeV)	R_I (fm)	a_I (fm)	V_{so}(MeV)	R_{so} (fm)	a_{so} (fm)
14	14	113.015	0.902	0.875	10.659	1.007	0.900	14.342	1.281	0.694
16	15	111.531	0.948	0.871	10.211	1.635	0.437	10.991	0.505	0.541
40	11	126.922	1.004	0.500	5.625	1.800	0.736	6.606	0.988	0.4038

Another source of higher order effects comes from explicit multistep excitations of the target. These targets are spherical but vibrate, and thus there are several possible couplings that could be considered within the coupled channel Born approximation (CCBA). Taking into account the nuclear deformation lengths determined from nucleon inelastic studies [42,43], we have included the excited state of the target that couples most strongly to the ground state, the 3^- state. Again the deuteron optical potential is refitted to reproduce the elastic scattering correctly. We find that for ^{14}C, these couplings have very little effect. This is not the case for both ^{16}O and ^{40}Ca.

Let us first consider ^{17}O. Its ground state is described in terms of a coupled-channel equation that generates a dominant $d_{5/2}$ component. Changing r_0 can have a dramatic effect in the structure composition (mixing in p- and f-waves), and thus one needs to limit the range of single particle parameters where a realistic structure is preserved. Results are shown in Table V. Including the coupling to the 3^- state, reduces the transfer cross section, increasing the SF. The resulting ANC of the $d_{5/2}$ for a unit SF, is 0.56 fm^{-1}.

In the ^{41}Ca case, the situation is different. Taking again only values of r_0 that generate coupled-channel wave functions for ^{41}Ca that are still dominantly $f_{7/2}$, one obtains transfer cross sections that are smaller than in the single particle case. Thus the extracted SFs are higher (see Table VI). Nevertheless, the ANCs associated with the $f_{7/2}$ component are still much smaller than the number extracted from the sub-Coulomb measurement. We have performed CRC iterations on CCBA calculations for ^{40}Ca$(d, p)^{41}$Ca at $E_d = 11$ MeV. In this case the transfer couplings involved are $d + {}^{40}\text{Ca(g.s.)} \rightarrow p + {}^{41}\text{Ca(g.s.)}$ and $d + {}^{40}\text{Ca}(3^-_1) \rightarrow p + {}^{41}\text{Ca(g.s.)}$, with spectroscopic factors as in Table VI. We find the picture does not change significantly.

E. DBWA with a simultaneous fit

It is impossible to rule out other excitation mechanisms which may contribute to the transfer process, however we do not expect these will be stronger than the ones discussed in Sec. III D. One interesting question is whether there would be any way of obtaining the desired consistency between SF and ANC within the simplified DWBA picture, specially in the ^{41}Ca case, where the mismatch is so large. We assume that we can introduce all higher order processes into a local effective deuteron optical potential. We impose that the SF for a neutron outside a closed shell be unity, and chose the single particle parameters such that they reproduce the ANC extracted from experiment (see Table VII). We perform a nine parameter fit of the deuteron optical potential to both the elastic and the transfer data. Our starting potential is that obtained in Sec. III B. The fit consists of a standard χ^2 minimization procedure and the code SFRESCO is used [36]. For each case we do find a potential that is able to reproduce the elastic

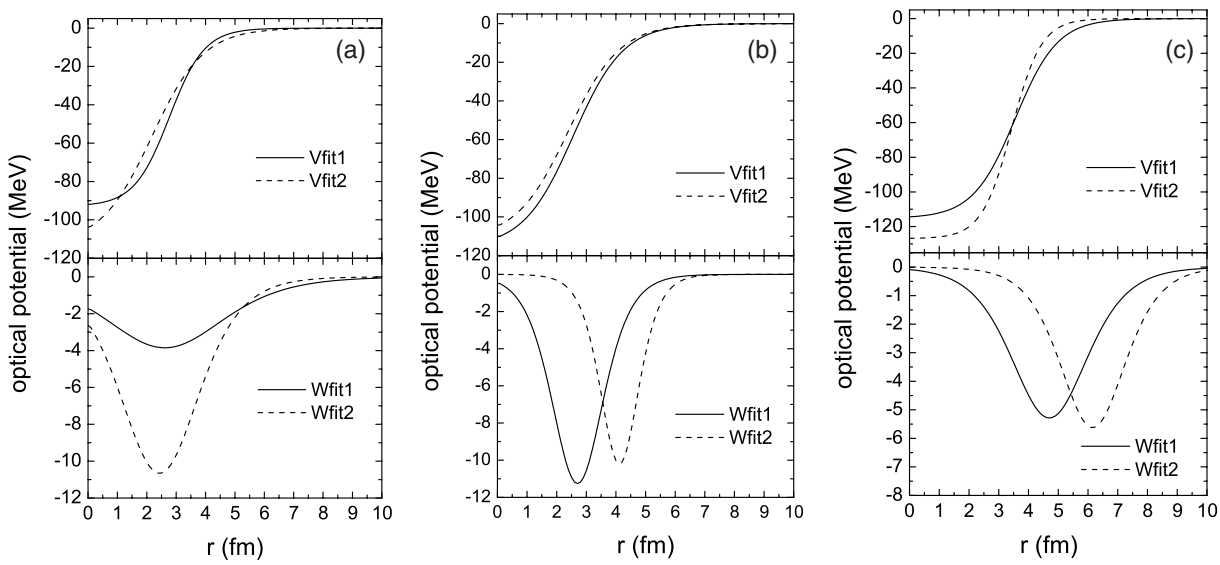

FIG. 10. Optical potentials: fits to elastic scattering only—real (Vfit1) and imaginary (Wfit1)—and simultaneous fits to the elastic and transfer channel—real (Vfit2) and imaginary (Wfit2). (a) $^{14}\text{C} + d$ at $E_d = 14$ MeV, (b) $^{16}\text{O} + d$ at $E_d = 15$ MeV, (c) $^{41}\text{Ca} + d$ at $E_d = 11$ MeV.

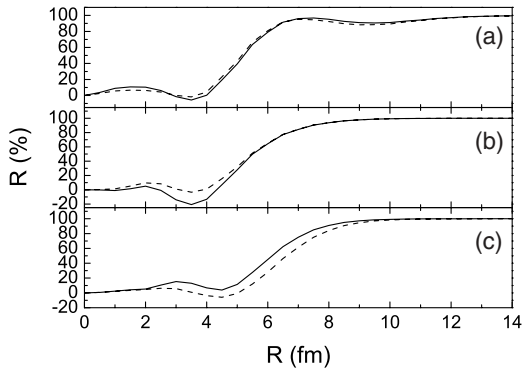

FIG. 11. Peripherality test for the reactions (using a cut in the radial distance between projectile and target): (a) $^{14}C + d$ at $E_d = 14$ MeV, (b) $^{16}O + d$ at $E_d = 15$ MeV, (c) $^{41}Ca + d$ at $E_d = 11$ MeV. The solid line corresponds to fit 1 potential and the dashed line to fit 2.

and the transfer simultaneously, under the constraint of SFs and ANCs. The resulting real (Vfit2) and imaginary (Wfit2) potentials from this fit are presented for all three reactions, as the dashed lines (*fit2*) in Fig. 10. The parameters are explicitly shown in Table VIII. The solid lines correspond to the previous elastic fit (*fit1*), whose parameters were shown in Table II. It appears that for $^{14}C + d$ at $E_d = 14$ MeV, the real part becomes slightly more diffuse, whereas for $^{41}Ca + d$ at $E_d = 11$ MeV, it becomes clearly less diffuse. The $^{16}O + d$ at $E_d = 15$ MeV case is rather unchanged, which reflects the fact that to start with the inconsistency in this case was minor. We find that the most significant change in the resulting potentials is an increase of the imaginary part in the surface region, which is obtained either by a large imaginary depth or by a shift toward the surface. This suggests that the standard DWBA is overestimating the surface contribution.

Changes in the deep interior do not reflect sensitivity of the transfer process to this region. Transfer reactions are known to be surface peaked. This usually means that impact parameters smaller than the sum of the projectile and target radii do not contribute to the reaction. In $A(d, p)B$, this is related to the cutoff on $\mathbf{R_{dA}}$. The results of this standard peripherality check is shown in Fig. 11 for the three reactions under study. The percentage ratio of the cross section integrated up to $R_{dA} = R$ to the total transfer cross section $R(\%)$ is plotted. In the deep interior this ratio is zero and it goes to 100% for large distances. The region where it increases rapidly corresponds to the surface region, where the transfer takes place.

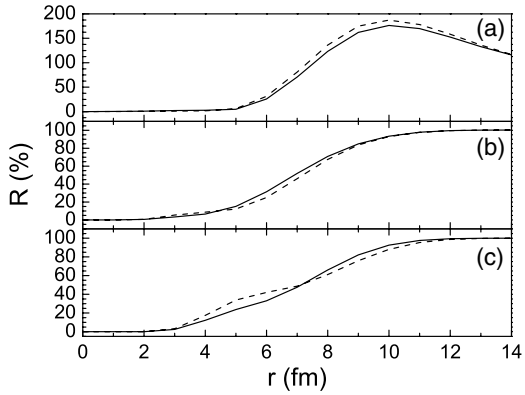

FIG. 12. Peripherality test for the reactions (using cutoff in the radial distance R_{nA}): (a) $^{14}C + d$ at $E_d = 14$ MeV, (b) $^{16}O + d$ at $E_d = 15$ MeV, (c) $^{41}Ca + d$ at $E_d = 11$ MeV. The solid line corresponds to fit 1 potential and the dashed line to fit 2.

However, to probe the sensitivity to the SF, one needs to analyze the dependence with $\mathbf{R_{nA}}$. Under a zero range approximation of the deuteron, these two tests would be identical. When taking into account the finite range of V_{np} and the remnant part of the full transition operator, peripherality in $\mathbf{R_{dA}}$ is not equivalent to peripherality in $\mathbf{R_{nA}}$. To illustrate this fact, peripherality tests were performed by evaluating the interior contribution to the total transfer cross section relative to $\mathbf{R_{nA}}$. These peripherality tests are based on DWBAf (*fit 1*) and DWBA with the deuteron potential fit simulaneously to elastic and transfer (fit 2). We take the radial integrals in the coordinates of R_{nA}, R_{pB}, and truncate the integration in R_{nA} to a maximum value r:

$$\frac{d\sigma}{d\Omega}(r) \sim \left(\int_0^{\infty} \int_0^{r} \psi_f^{(-)} I_{An}^{B} \Delta V \varphi_{pn} \psi_i^{(+)} \mathbf{dR_{nA}} \mathbf{dR_{Bp}} \right)^2. \quad (4)$$

The percentage ratio of this value to the full integration is presented in Fig. 12. As before, if $r = 0$ fm, the ratio should be zero, and it should tail off at 100% when r becomes very large. Results show that, in all cases there is no contribution up to 2 fm. One can also see that, even though 14 MeV is above the Coulomb barrier, the $^{14}C(d, p)$ happens at rather large distances, due to its loosely bound nature. Contributions up to 20% from the surface/interior are present in both $^{16}O + d$ at $E_d = 15$ MeV and $^{41}Ca + d$ at $E_d = 11$ MeV.

IV. DISCUSSION AND CONCLUSIONS

In this work we have studied transfer reactions to states considered good single particles, with three different Q-values, namely $^{14}C(d, p)^{15}C$(g.s.) at $E_d^{\text{lab}} = 14$ MeV, $^{16}O(d, p)^{17}O$(g.s.) at $E_d^{\text{lab}} = 15$ MeV $^{40}Ca(d, p)^{41}Ca$(g.s.) at $E_d^{\text{lab}} = 11$ MeV. All these reactions are above the Coulomb barrier and therefore contain some information from the interior. The standard DWBA method, using global optical potentials and the typical single particle parameters, produces SFs in agreement with shell model predictions, however the corresponding ANCs are not consistent with those extracted from independent measurements. If one imposes, within the DWBA formulation, ANCs that are consistent with the experimental values, the extracted SFs are significantly reduced compared to the shell model predictions.

Some improvements on the SF/ANC mismatch can be obtained by using a deuteron optical potential fitted directly to the corresponding elastic data, at the relevant energy. In particular, for $^{16}O(d, p)$ we obtain SF/ANC consistency. However the problem for the other two cases is not resolved. The deuteron adiabatic potential, which takes into account breakup, can change the SF up to 30%. This improves the situation for $^{14}C(d, p)$ but fails to bring the ^{41}Ca ANC

anywhere close to the value extracted from an independent sub-Coulomb measurement.

Deuteron breakup is not the only important ingredient to the solution of this problem: in all cases we find an influence of surface higher order effects. For ^{14}C$(d, p)^{15}$C(g.s.) at $E_d^{\rm lab} = 14$ MeV, CCBA effects are negligible but CRC effects produce a reduction of the ANC consistent with unity SF: $C^2 = 2.14$ fm^{-1}, a significant reduction compared to the DWBA case, which together with the reduction from deuteron breakup produces an ANC much closer to the experimental value $C^2 = 1.48 \pm 0.18$ fm^{-1}. For ^{16}O$(d, p)^{17}$O(g.s.) at $E_d^{\rm lab} = 15$ MeV, CRC effects are small but CCBA couplings to the 3^- state in ^{16}O were found to be important. This brings down the C^2 from 0.76 to 0.56, neither too far from the experimental number 0.67 ± 0.05 fm^{-1}. Finally, the ^{40}Ca$(d, p)^{41}$Ca(g.s.) case remains problematic: both CRC and CCBA are relevant but act in the wrong direction. Overall, an ANC, consistent with unity SF, falls short by nearly a factor of 2.

Contrary to $(e, e'p)$ measurements, transfer reactions are surface peaked and it is disconcerting that the traditional methods to handle higher order effects at the surface are not able to solve the SF/ANC discrepancy for one of our test cases. The very fact that, even when the energies are well above the Coulomb barrier, there is such a large contribution from the peripheral region, makes it extremely important to pin down the ANC input unambiguously. We cannot rule out the possibility of a problem in the ^{41}Ca ANC we extracted from other data. Experiments to measure ANCs for this case are crucial to settle this matter. In the future we suggest that experiments be designed for the extraction of ANCs in parallel with the corresponding experiments aimed at extracting SFs.

ACKNOWLEDGMENTS

This work was supported by the National Science Foundation, under Grant No. PHY-0456656 and the U.S. Department of Energy, under Grant No. DE-FG02-93ER40773. D.Y.P. acknowledges the support of the National Superconducting Cyclotron Laboratory during his visit.

[1] B. A. Brown, P. G. Hansen, B. M. Sherrill, and J. A. Tostevin, Phys. Rev. C **65**, 061601(R) (2002).
[2] R. B. Wiringa, Presentation at the Workshop on New perspectives on p-shell nuclei—the nuclear shell model and beyond, Michigan State University, 22–24 July 2004 (http://www.nscl.msu.edu/∼brown/p-shell-2004/index.html).
[3] L. Lapikás, J. Wesseling, and R. B. Wiringa, Phys. Rev. Lett. **82**, 004404 (1999).
[4] S. A. Goncharov *et al*., Sov. J. Nucl. Phys. **35**, 383 (1982).
[5] N. Austern, *Direct Nuclear Reaction Theories* (Wiley, New York, 1970).
[6] J. Al-Khalili and F. Nunes, J. Phys. G: Nucl. Part. Phys. **29**, R89 (2003).
[7] G. J. Kramer, H. P. Blok, and L. Lapikas, Nucl. Phys. **A679**, 267 (2001).
[8] C. Barbieri and L. Lapikás, Phys. Rev. C **70**, 054612 (2004).
[9] A. Navin *et al*., Phys. Rev. Lett. **81**, 5089 (1998).
[10] A. Gade *et al*., Phys. Rev. Lett. **93**, 042501 (2004).
[11] P. G. Hansen and J. A. Tostevin, Annu. Rev. Nucl. Part. Sci. **53**, 219 (2003).
[12] R. J. Furnstahl and H.-W. Hammer, Phys. Lett. **B531**, 203 (2002).
[13] J. P. Schiffer *et al*., Phys. Rev. **164**, 1274 (1967).
[14] X. Tang *et al*., Phys. Rev. C **69**, 055807 (2004).
[15] C. Iliadis and M. Wiescher, Phys. Rev. C **69**, 064305 (2004).
[16] X. D. Liu, M. A. Famiano, W. G. Lynch, M. B. Tsang, and J. A. Tostevin, Phys. Rev. C **69**, 064313 (2004).
[17] M. B. Tsang, J. Lee, and W. G. Lynch, Phys. Rev. Lett. **95**, 222501 (2005).
[18] F. Delaunay, F. M. Nunes, W. G. Lynch, and M. B. Tsang, Phys. Rev. C **72**, 014610 (2005).
[19] J. Lee, J. A. Tostevin, B. A. Brown, F. Delaunay, W. G. Lynch, M. J. Saelim, and M. B. Tsang, Phys. Rev. C **73**, 044608 (2006).
[20] A. M. Mukhamedzhanov and F. M. Nunes, Phys. Rev. C **72**, 017602 (2005).
[21] M. A. Franey *et al*., Nucl. Phys. **A324**, 193 (1979).
[22] S. Burzynski *et al*., Nucl. Phys. **A399**, 230 (1983).
[23] E. Sauvan *et al*., Phys. Rev. C **69**, 044603 (2004).
[24] V. Maddalena *et al*., Nucl. Phys. **A682**, 332c (2001).
[25] Texas A&M Progress report 2001–2002, pp. 1–6.
[26] N. K. Timofeyuk, D. Baye, P. Descouvemont, R. Kamouni, and I. J. Thompson, Phys. Rev. Lett. **96**, 162501 (2006).
[27] H. Schär, D. Trautmann, and E. Baumgartner, Helv. Phys. Acta **50**, 29 (1977).
[28] R. L. Varner *et al*., Phys. Rep. **201**, 57 (1991).
[29] R. C. Johnson and P. J. R. Soper, Phys. Rev. C **1**, 055807 (1970).
[30] V. Reid, Ann. Phys. (NY) **50**, 411 (1968).
[31] C. M. Perey and F. G. Perey, At. Data Nucl. Data Tables **17**, 1 (1976).
[32] J. D. Goss *et al*., Phys. Rev. C **12**, 1730 (1975).
[33] E. L. Keller, Phys. Rev. **121**, 820 (1961).
[34] D. C. Kocher and W. Haeberli, Nucl. Phys. **A172**, 652 (1971).
[35] http://groups.nscl.msu.edu/nscl_library/pddp/database.html
[36] I. J. Thompson, Comput. Phys. Rep. **7**, 167 (1988).
[37] C. E. Busch *et al*., Nucl. Phys. **A223**, 183 (1974).
[38] C. C. Foster, Phys. Rev. **181**, 1529 (1969).
[39] Y. Sakuragi, M. Yahiro, and M. Kamimura, Prog. Theor. Phys. Suppl. **89**, 136 (1986).
[40] G. L. Wales and R. C. Johnson, Nucl. Phys. **A274**, 168 (1976).
[41] R. C. Johnson, in *Proceedings of the Second Argonne/MSU/JINA/INT RIA Workshop on Reaction Mechanisms for Rare Isotope Beams*, edited by B. A. Brown, AIP Conf. Proc. No. 791 (AIP, New York, 2005), p. 128.
[42] S. Raman, C. W. Nestor, and P. Tikkanen, At. Data Nucl. Data Tables **78**, 1 (2001).
[43] T. Kibedi and R. H. Spear, At. Data Nucl. Data Tables **80**, 35 (2002).